Fluid Dynamics Research 8 (1991) 85–100
North-Holland

FLUID DYNAMICS
RESEARCH

Analysis of turbulent flows by means of the empirical eigenfunctions

Lawrence Sirovich

Center for Fluid Mechanics and The Division of Applied Mathematics, Brown University, Providence, RI 02912, USA

Received 10 October 1990; revised manuscript received 24 April 1991

Abstract. The method of empirical eigenfunctions is developed in a general framework. In particular it is shown that the *method of snapshots* leads to the determination of the empirical eigenfunctions in any number of dimensions in terms of an equivalent one-dimensional problem. The methodology is discussed within the framework of some turbulent simulations and it is shown how this facilitates the flow analysis. In another vein it is demonstrated that the empirical eigenfunctions lead to a generalization of the Kolmogorov inertial range theory. Finally we discuss the application of the empirical eigenfunctions to the determination of low-dimensional dynamical systems. Some speculations on future directions are also mentioned.

1. Introduction

In keeping with the theme of the workshop I will discuss *novel (numerical) experiments and data processing for the better understanding of turbulence*. At the heart of the following presentation is the Karhunen–Loéve [1,2] (KL) procedure for generating the empirical eigenfunctions. In a well-defined sense these functions lead to an optimal description of turbulent flows. They also provide a system of coordinate functions which are intrinsic to the particular flow geometry and regime.

Lumley [3] suggested more than twenty years ago that the KL procedure [#1] should be used to unambigously and rationally extract coherent structures in a turbulent flow. (Also see refs. [4,5].) While this use of the empirical eigenfunctions still needs to be established [6], the procedure is of unquestioned value in treating and analyzing turbulent flows. Since Lumley's original paper the KL procedure has figured in a number of studies [7–9], however it is only in recent times that the KL procedure has begun to realize its full potential for dealing with turbulent flows as generated in the laboratory or on the computer. One of the reasons for the long delay is that only in recent times have we been able to create data bases massive enough to satisfy the appetite of the KL procedure. Another, and perhaps more compelling reason was the erroneous notion that the method could not be extended beyond one-dimensional data bases or their equivalents. However, this misconception was dispelled by the *method of snapshots* [10–12] which demonstrated that the empirical eigenfunctions of fully three-dimensional flows, of arbitrary resolution, could be calculated essentially without approximation. We begin in the next section with a presentation of these ideas.

[#1] Lumley, following Loéve, referred to this as the proper orthogonal decomposition (POD).

2. The method of snapshots

Since the KL procedure is textbook material [13–15] no attempt will be made to derive the procedure in detail. Nevertheless the presentation which follows is somewhat novel and represents a point of view not fully recognized in the literature.

Imagine a flow characterized by a vector

$$\boldsymbol{v} = \boldsymbol{v}(\boldsymbol{x}, t), \tag{1}$$

which may be the three components of velocity or a more complicated field vector including for example temperature, salinity and so forth if required. Further we assume an inner product, $(\boldsymbol{v}, \boldsymbol{v}')$, for example

$$(\boldsymbol{v}, \boldsymbol{v}') = \int_V \sum_k v_k(\boldsymbol{x}, t) v_k'(\boldsymbol{x}, t)\, \mathrm{d}\boldsymbol{x}, \tag{2}$$

where V is the volume of the domain of interest. We also assume a norm, which for convenience we take to be based on the inner product (2),

$$\| \boldsymbol{v} \|^2 = (\boldsymbol{v}, \boldsymbol{v}) \tag{3}$$

and, finally, we assume the existence of an averaging process $\langle\ \rangle$, which for example might be given by the time average,

$$\langle \phi \rangle_T = \frac{1}{T} \int_{-T/2}^{T/2} \phi(t)\, \mathrm{d}t. \tag{4}$$

Now that the three forms (2), (3) and (4) have been defined, we emphasize that these specific forms need not be employed in the following, and that the results that are presented depend specifically on the inner product, norm and averaging procedure which have been adopted.

In order to characterize or represent the flow (1) in general, one can employ an admissible complete orthonormal basis set $\{\boldsymbol{\phi}^{(n)}\}$. By admissible we mean that the $\boldsymbol{\phi}^{(n)}(\boldsymbol{x})$ satisfy boundary and other possible conditions, e.g., if the flow is incompressible we require that

$$\nabla \cdot \boldsymbol{\phi}^{(n)} = 0, \tag{5}$$

for admissibility. On practical grounds we can represent a flow, eq. (1), only in terms of a finite set of functions,

$$\boldsymbol{v} \approx \boldsymbol{v}_N = P_N \boldsymbol{v} = \sum_{k=1}^{N} a_k(t) \boldsymbol{\phi}^{(k)}(\boldsymbol{x}). \tag{6}$$

In geometrical terms, $\boldsymbol{v}$ is being approximated by a point $\boldsymbol{v}_N$ lying in an N-dimensional hyperplane. As is easily seen the best approximation in the sense of the norm, eq. (3), is obtained when the time dependent coefficients are the Fourier coefficients,

$$a_k = (\boldsymbol{\phi}^{(k)}, \boldsymbol{v}). \tag{7}$$

In other words, when $\boldsymbol{v}_N$ lies at the foot of the perpendicular from $\boldsymbol{v}$ to the hyperplane. This is already implied by the use for the projection operator P_N in eq. (6) The representation (6) and in particular the error

$$\epsilon_N = \| \boldsymbol{v} - \boldsymbol{v}_N \|^2 = \| \boldsymbol{v} \|^2 - \| \boldsymbol{v}_N \|^2 \tag{8}$$

depend on the particular choice of the basis set $\{\boldsymbol{\phi}^{(n)}\}$. In general there exist an infinite variety of admissible basis sets. According to the KL theorem there exists a unique basis set (up to choices within degenerate invariant subspaces) such that

$$\lim_{T \uparrow \infty} \langle \epsilon_N \rangle_T = \bar{\epsilon}_N \tag{9}$$

is a minimum for any N. With this basis the N-dimensional hyperplane, on average, is the most proximate to v. The distinguished set of functions is termed the *empirical eigenfunctions*. It should be emphasized again, that this choice of a basis set depends on the selection of inner product, norm and average. However in order to avoid the complications of a general presentation, in what follows we use eqs. (2), (3) and (4) for these quantities.

Since ϵ_N in eq. (9) is a quadratic form, it follows that the empirical eigenfunctions are given by a linear integral equation, viz.

$$\int_V \mathrm{d}y\, \mathbf{K}(x, y)\phi(y) = \lambda\phi(x), \tag{10}$$

where the components of the matrix kernel $\mathbf{K}$ are given by,

$$K_{jk} = \frac{1}{T}\int_{-T/2}^{T/2} v_j(x, s)v_k(y, s)\,\mathrm{d}s. \tag{11}$$

$\mathbf{K}$ is a non-negative, hermitian kernel which on physical grounds can be expected to be square integrable. [Here, and in the following we avoid the additional notation of taking the limit as $T \uparrow \infty$, since in actual practice this is never carried out.]

It is worth pausing at this point to comment briefly on the nature of the empirical eigenfunctions. We see that these furnish an optimal set of *fitting* functions for the phenomenon in the sense that the averaged error, eq. (9), is minimal for all N. This property is achieved by generating functions that are *intrinsic* to the details of the problem, and that depends on knowing the flow. It is also worth commenting on the fact that although in general v arises from a nonlinear process, eq. (10) appears to reformat the description in terms of a basis set $\{\phi^{(n)}\}$ generated by a linear process. This should not convey to the reader the notion that the problem has in any way been linerarized. For the kernel $\mathbf{K}$ from which the eigenfunctions have been obtained is itself the result of a nonlinear process. In geometric terms, eqs. (6) and (7) state that the best approximation to v in terms of an N-dimensional hyperplane is gotten by orthogonal projection. The empirical eigenfunctions then furnish, on average, the closest hyperplane to v.

To solve for the eigenfunctions we observe that $\mathbf{K}$, eq. (11), bears a formal resemblance to a degenerate kernel and hence we can seek a solution in the form

$$\phi(x) = \int_{-T/2}^{T/2} \mathrm{d}s\, \alpha(s)v(x, s), \tag{12}$$

i.e. an admixture of the instantaneous flow fields in the interval $(-T/2, T/2)$, as determined by the relative strengths, $\alpha(s)$. As a result we have referred to this as the method of snapshots [10]. From this it easily follows that a necessary condition for solution is

$$\int_{-T/2}^{T/2} C(t, s)\alpha(s)\,\mathrm{d}s = \lambda\alpha(t), \tag{13}$$

where

$$C(t, s) = C(s, t) = T^{-1}(v(s), v(t)). \tag{14}$$

On a practical note eq. (13) is solved numerically by sampling the flow at discrete times so that eq. (13) reduces to the eigentheory of a symmetric matrix gotten from sampling $C(t, s)$ in s and t. As a rule it is prudent to sample C at uniform times which are comparable to or larger than the autocorrelation time.

In regard to the autocorrelation it is important to observe that $C(t, s)$ is *not* the autocorrelation. In particular, consider eq. (14) and imagine that $v(x, t)$ explores a chaotic attractor. Then for s fixed and t increasing, the value of $C(t, s)$ tends to zero and remains near zero for the

most part since eq. (14) represents the inner product of uncorrelated fields. However under the assumption of boundedness and ergodicity, $\boldsymbol{v}(\boldsymbol{x}, t)$ will come arbitrarily close to $\boldsymbol{v}(\boldsymbol{x}, s)$ as time evolves. At such times (14) is relatively large. Thus unlike the autocorrelation, $\mathscr{C}(t-s)$, which can be obtained by taking the ensemble average of (14), $C(t, s)$, *does not* vanish for $|t-s|$ large. Analytically the difference is seen in the two following forms,

$$\mathscr{C}(t-s) = \int \exp[\mathrm{i}\omega(t-s)](\tilde{\boldsymbol{v}}(\omega), \tilde{\boldsymbol{v}}(\omega))_{\mathrm{e}}\, \mathrm{d}\omega, \tag{15}$$

and

$$C(t, s) = \int \mathrm{d}\omega\, \mathrm{d}\omega' \exp(\mathrm{i}\omega t - \mathrm{i}\omega' s)(\tilde{\boldsymbol{v}}(\omega), \tilde{\boldsymbol{v}}(\omega')) \tag{16}$$

in terms of the Fourier transform

$$\tilde{\boldsymbol{v}}(\omega) = \int \exp(-\mathrm{i}\omega t)\boldsymbol{v}(x, t)\, \mathrm{d}t. \tag{17}$$

In eq. (15), the subscript e indicates that a suitable ensemble average has been performed.

Another observation is that the *Fourier coefficients* a_k, eq. (7), and the eigenfunctions α, eq. (13), are simply proportional to one another,

$$\alpha_k = a_n/\lambda_n T. \tag{18}$$

To see this we formally write

$$\boldsymbol{v}(\boldsymbol{x}, t) = \sum a_n(t)\boldsymbol{\phi}^{(n)}(\boldsymbol{x}), \tag{19}$$

where a_n is given by eq. (7). If we denote by $\alpha_k(t)$ the functional form in eq. (13) that corresponds to $\boldsymbol{\phi}^{(k)}$ in eq. (12), then eq. (19) yields

$$\int_{-T/2}^{T/2} \alpha_k(t)\boldsymbol{v}(\boldsymbol{x}, t)\, \mathrm{d}t = \boldsymbol{\phi}^{(k)}(\boldsymbol{x}) = \sum \int_{-T/2}^{T/2} \alpha_k(t) a_n(t)\, \mathrm{d}t\, \boldsymbol{\phi}^{(n)}(x)$$

from which eq. (18) directly follows.

It follows from the symmetry of $C(t, s)$, (14), and (18) that

$$\langle a_n a_m \rangle = \langle (\boldsymbol{\phi}^{(n)}, \boldsymbol{v})(\boldsymbol{\phi}^{(m)}, \boldsymbol{v}) \rangle = \lambda_n \delta_{nm}. \tag{20}$$

Thus the effect of utilizing the empirical eigenfunctions is to produce a representation in which the Fourier coefficients are decorrelated. On average the Fourier modes do not interact (although short-term interaction, in general, is to be expected). In this regard the empirical eigenfunctions are unique (up to fine print about invariant subspace) amongst all admissible orthonormal systems. It may be shown that eq. (20) is a necessary and sufficient condition for the error, eq. (9), to be a minimum.

3. Rayleigh–Bénard convection—a brief summary

The method of empirical eigenfunctions, as described in the previous section, has been applied to computational simulations based on the Ginzburg–Landau equation [16], Rayleigh–Bénard convection [17–21], channel flow [22] as well as to an experimental investigation of the turbulent jet [23].

The most thoroughly investigated case is that of Rayleigh–Bénard convection. The case considered was that of a fluid contained between infinite parallel planes, perpendicular to the vertical or z-direction. The temperature is prescribed on the bounding planes which are taken

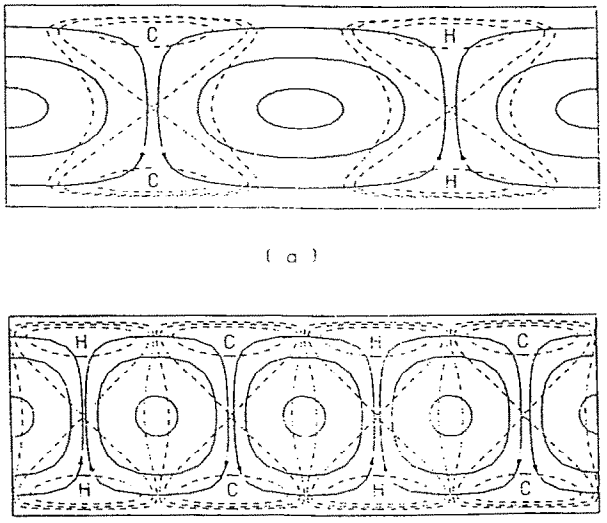

Fig. 1. (a) Streamlines (continuous curves) and isotherms (dashed curves) for $\phi_{01}^{(1)}$. (b) Same as (a) for $\phi_{11}^{(1)}$, but viewed on a diagonal of the square plane form.

to be stress free. Periodicity is assumed in the horizontal or x, y-directions. As a result of the homogeneity of the problem in the horizontal directions the eigenfunctions are factorable,

$$\phi = \Phi_{kl}^{(q)}(z)\,\exp[\mathrm{i}2\pi(kx + ly)/L] = \phi_{kl}^{(q)}, \tag{21}$$

where L is the aspect ratio, width to height. [In order to increase the symmetries the planform was taken to a square.] k and l are horizontal wavenumbers and q denotes the vertical *quantum number*.

In fig. 1 we show the first two most energetic eigenfunctions. Figure 1a shows $\phi_{01}^{(1)}$ which is a two-dimensional rolling motion, indicated by the streamlines, which lifts heated fluid and drops cooled fluid, as indicated by the isotherms. This mode is four-fold degenerate – the eigenfunction may be displaced by a quarter wavelength in the horizontal and also rotated by $\pi/2$ about a vertical axis. The second eigenfunction $\phi_{11}^{(1)}$, the streamlines of which are indicated in fig. 1b, is composed of four rolls aligned along a diagonal, and for the reasons already given, it too is four-fold degenerate.

All calculations have been based on simulations of the Boussinesq equations [24]. Two cases have received the most thorough study $\mathrm{Ra}/\mathrm{Ra}_c = 70$ [17] and $\mathrm{Ra}/\mathrm{Ra}_c = 9800$ [18,19]. The first lies in the soft turbulence regime and the second in the hard turbulence regime as defined by the Chicago group [25]. (For a parametric study of the eigenfunctions and related questions, at

Table 1

$\mathrm{Ra} = 70\mathrm{Ra}_c$						$\mathrm{Ra} = 9.8\times10^3\mathrm{Ra}_c$					
n	q	k_x	k_y	deg	% energy	n	q	k_x	k_y	deg	% energy
1	1	0	1	4	41.04	1	1	0	1	4	24.56
2	1	1	1	4	8.87	2	1	1	1	4	3.23
3	2	0	1	4	4.23	3	2	0	1	4	2.00
4	1	0	0	2	1.67	4	1	1	2	8	0.95
5	1	0	2	4	2.82	5	1	0	2	4	0.71

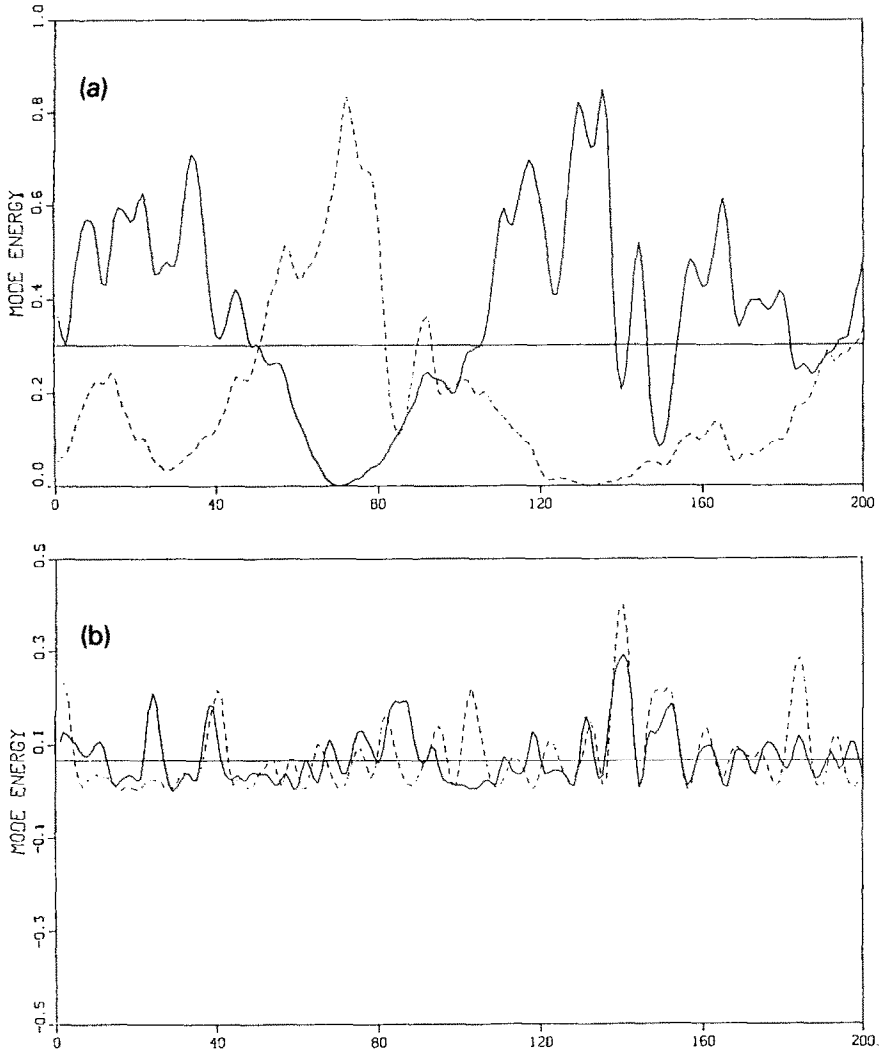

Fig. 2. (a) Time histories of the amplitudes of the $(\phi_{01}^{(1)}, \phi_{0-1}^{(1)})$ roll (continuous curve) and $(\phi_{10}^{(1)}, \phi_{-10}^{(1)})$ roll (dashed curve). (b) Same as (a) for the case corresponding to fig. 1b.

low Ra see refs. [26,27].) Table 1 indicates the average energy of the first 5 modes for each of the two cases.

At the lower Rayleigh number more than 40% of the energy is taken up by the roll motion depicted in fig. 1. Even at the very high value of Ra almost 25% of the energy is still in this mode. [We see that mode crossing first occurs at $n = 4$.] Both instances strongly underline the fact that the empirical eigenfunctions optimally organize the data. The fact that even in the hard turbulence regime a quarter of the energy, on average, is in the form of a simple rolling motion may be helpful in understanding this complicated flow.

Figure 2 shows the time course of the corresponding coefficients $a_{01}^{(1)}$ and $a_{11}^{(1)}$. [As shown in the previous section these coefficients are eigenfunctions of the kernel (14).] The rolls seemingly at random times rotate about the vertical axis by $\pi/2$. They also undergo sidewise shifts, or jitter, in addition to these rotations.

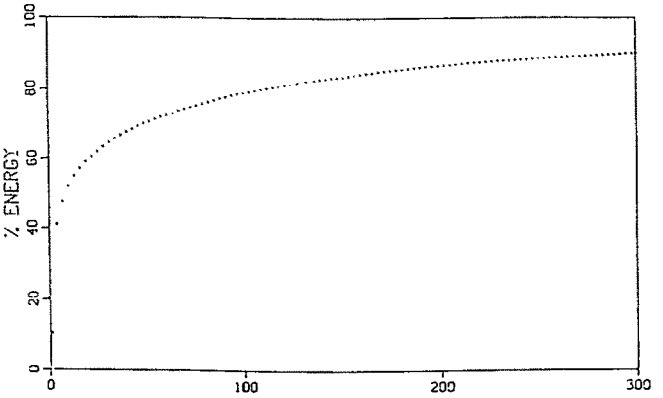

Fig. 3. Per cent of energy captured versus the number of modes, for $\mathrm{Ra} = 70\mathrm{Ra}_c$.

The results indicated in the table are also significant for the purpose of data compression. For example for $\mathrm{Ra} = 70\mathrm{Ra}_c$, 80% of the average energy is captured by 106 terms, 90% by 289 terms and 95% by 608 terms. This is summarized in fig. 3 for $\mathrm{Ra}/\mathrm{Ra}_c = 70$.

4. Inertial range theory for inhomogeneous turbulence

Kolmogorov [28] introduced the concept of an inertial range in turbulence as being *that part of the energy spectrum neither directly affected by the external sources creating the flow nor by viscous dissipation*. In the course of developing his theory it was necessary for Kolmogorov to require that the turbulence be homogeneous and isotropic at least in some sense. For purposes of exposition we briefly review Kolmogorov's development.

If we consider the average energy e, then we can write,

$$e = \frac{1}{V}\int_V \langle v^2 \rangle_e \, \mathrm{d}\boldsymbol{x} = \int \mathscr{E}(\boldsymbol{k}) \, \mathrm{d}\boldsymbol{k} = \int \mathscr{E}(k) 4\pi k^2 \, \mathrm{d}k = \int E(k) \, \mathrm{d}k. \tag{22}$$

The second integral, which defines energy per volume of wavenumber space, $\mathscr{E}(\boldsymbol{k})$, is a consequence of homogeneity. The third and fourth integrals which define the energy in a spherical shell of wavenumber space, $E(k)$, is a consequence of isotropy. To obtain the Kolmogorov result characterizing the energy spectral density in the inertial range we note that the full functional dependence of E is

$$E = E(k, H, U, \nu), \tag{23}$$

where H and U are the integral length and velocity scales and ν the kinematical viscosity. [If we turn our back, for the moment, on the assumptions of homogeneity and isotropy then for channel flow H is the channel height and $U = (H\,|\partial P_0/\partial x\,|/\rho)^{1/2}$, where $\partial P_0/\partial x$ is the external pressure gradient.] If we define

$$\epsilon = U^3/H, \quad \kappa = (\epsilon/\nu^3)^{1/4} = 1/\eta, \tag{24}$$

where ϵ is referred to as the *energy flux* and η as the Kolmogorov microscale [29], it then follows from the Buckingham Π-theorem [30] that

$$\frac{E}{\epsilon^{2/3}k^{-5/3}} = f(k/(1/H), k/\kappa). \tag{25}$$

[Note that the Reynolds Re number is still present since the ratio of the first to the second argument of f gives $H\kappa = \mathrm{Re}^{3/4}$.] Next, under the *inertial range limit*, defined by

$$1/H \ll k \ll \kappa, \tag{26}$$

provided f is well behaved, it follows that,

$$E \propto \epsilon^{2/3} k^{-5/3}, \tag{27}$$

which is the famous Kolmogorov result. Kolmogorov next invokes the concept of *local homogeneity and isotropy* in order to apply eq. (27), locally, to flows at sufficiently high Re. [It should be noted that Kolmogorov's argument was originally presented within the framework of physical space [28].]

This theory was later amended by Kolmogorov [31] in response to the criticism that it did not account for intermittency. The effect of intermittency was also considered by Mandelbrot [32] and Frisch et al. [33]. The consequences of intermittency has been reviewed by Frisch [34]. Although this issue plays no essential role here, we point out that its affect can be included within the framework of dimensional reasoning. If intermittency is factored into the argument then one obtains instead of eq. (27),

$$E \propto \epsilon^{2/3} k^{-5/3} k^{\delta}. \tag{28}$$

[See Frisch [34] for an interpretation of δ.] In order to arrive at eq. (27) it was assumed that f in eq. (25) is non-singular under the limit (26). Thus, to obtain eq. (28) it is only necessary to suppose that the limit is appropriately singular in one or both of the arguments. For example, if the inertial range is to be free of viscosity the likely singular limit is in the first argument of (25). Nevertheless, the Kolmogorov argument is still *marred* by the fact that the integral scale then has to appear in eq. (28), and the italicized phrase at the outset of this section is not strictly valid.

In order to relax the assumptions of homogeneity and isotropy we require a generalization of the energy densities that appear in eq. (22). This can be done within the framework of the empirical eigenfunctions [35]. As a starting point we return to the definition (11) of the kernel $\mathbf{K}(x, y)$. In terms of the empirical eigenfunctions the kernel has the spectral representation

$$\mathbf{K}(x, y) = \sum \lambda_n \boldsymbol{\phi}^{(n)}(x) \otimes \boldsymbol{\phi}^{(n)}(y), \tag{29}$$

where $\otimes$ signifies the outer product. From this we can complete

$$\int_V \langle v^2 \rangle_e \, \mathrm{d}x = \hat{e} = \mathrm{Tr}\, \mathbf{K} = \sum_n \lambda_n, \tag{30}$$

which is the average energy

$$\dim[\hat{e}] = \dim[\lambda_n] = l^5/t^2. \tag{31}$$

[Note that in case of Rayleigh–Bénard convection the *energy* also includes the square of the perturbed temperature.] From the discussion in section 2, in particular eq. (20), it follows that an eigenvalue λ_n represents the average part of the energy of the flow in the *direction* $\boldsymbol{\phi}^{(n)}$. The summation (29) is therefore a natural generalization of the energy integral in Fourier space for homogeneous turbulence, and the eigenvalues are the counterparts to $\mathscr{E}(\boldsymbol{k})$, the energy density per unit volume in wavenumber space that appears in eq. (22).

For plane channel flow, unbounded in the horizontal directions, the eigenfunctions take on the same form, eq. (21), as those mentioned in the previous section for RB convection. The corresponding eigenvalues, which are now regarded as the discrete version of the energy density, have the form (L is a spanwise length scale)

$$\lambda = \lambda^{(q)}(k_x, k_y, U, L, H, \nu). \tag{32}$$

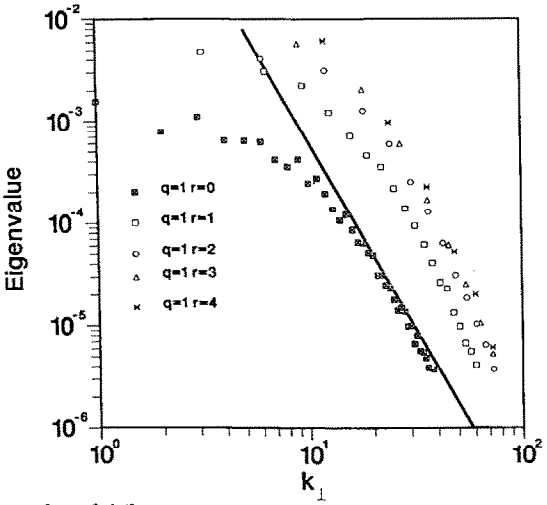

Fig. 4. $\lambda^{(q)}(k_x, k_y)$ versus $k_\perp = (k_x^2 + k_y^2)^{1/2}$ for the Kim, Moin and Moser [36] simulation of channel flow. The heavy continuous line represents a $k_\perp^{-11/3}$ dependence (see text).

Application of the Π-theorem yields

$$\frac{\lambda^{(q)}}{\epsilon^{2/3}k_\perp^{-11/3}} = F_q\big(k_\perp/(1/H),\ k_\perp/\kappa,\ k_y/k_x,\ H/L\big), \tag{33}$$

where

$$k_\perp = \sqrt{k_x^2 + k_y^2}\,. \tag{34}$$

Note that the denominator in eq. (34) is different than in eq. (25) because of eq. (31). Under the inertial range limit (26) we obtain

$$\lambda^{(q)} \propto \epsilon^{2/3}k_\perp^{-11/3} f^{(q)}\big(k_y/k_x\big) = \epsilon^{2/3}k_\perp^{-11/3} f^{(q)}(r). \tag{35}$$

[The geometric factor H/L has been suppressed in eq. (35).] In writing eq. (35) we have not assumed that isotropy is approached when $k_\perp/H^{-1} \to \infty$. In fig. 4 we examine the database generated by Kim et al. [36] for the modest value of Re = 3300, based on channel half width. Only the first quantum number is considered and a sequence of orientations. A relatively small but definite inertial range is seen to be present. On the other hand the original one-dimensional spectra in ref. [36] shows no indication of an inertial range. Figure 4 also implies that isotropy is not being approached. The case $r = 1$ is a factor of 8 greater than $r = 0$, with no indication that the two curves converge.

For the case of the RB convection, considered in section 3, it follows from dimensional reasoning that an eigenvalue has the form

$$\lambda = \lambda^{(q)}\big(k_x,\ k_y;\ \alpha,\ \nu,\ k,\ g,\ H,\ L\big), \tag{36}$$

where L is the diameter of the cell, H is the height of the convection cell, g is the gravitational constant, k is the thermal diffusivity, ν is the kinematical viscosity and $\alpha = \Delta T/T_0$ is the temperature ratio indicating the level of incremental heating of the convection cell. To facilitate use of the Π-theorem we introduce

$$\delta = H/\mathrm{Ra}^{1/3} = 1/\kappa, \tag{37}$$

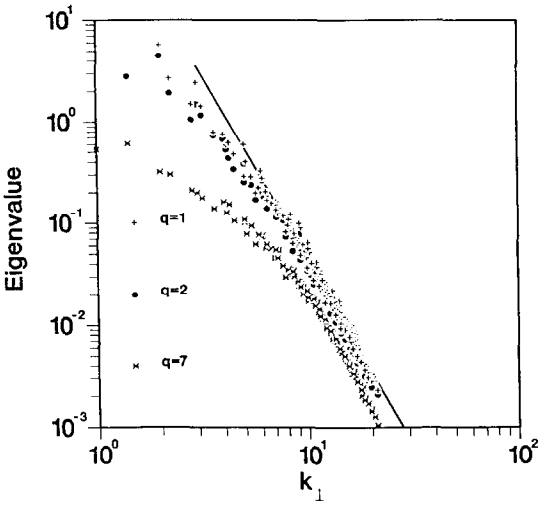

Fig. 5. Same as fig. 4 but for the case of RB convection in the hard turbulence regime [18,19].

which is an estimate of the thermal sublayer thickness and is the analogue of the Kolmogorov scale, η, in eq. (24). The relevant velocity of the flow is then given by

$$U = \sqrt{\alpha g \delta}\,. \tag{38}$$

From this and H and ϵ, eq. (24) is defined and if we proceed as before, then the Π-theorem yields

$$\frac{\lambda^{(q)}}{\epsilon^{2/3} k_{\perp}^{-11/3}} = F_q\big(k_{\perp}/(1/H),\ k_{\perp}/\kappa,\ k_y/k_x,\ \mathrm{Pr},\ \alpha,\ H/L\big). \tag{39}$$

Under the inertial range limit the dependence on $r = k_y/k_x$ dissapears since there is now no preferred horizontal direction and we obtain

$$\lambda^{(q)} \propto \epsilon^{2/3} k_{\perp}^{-11/3}, \tag{40}$$

where the dependence on geometry, H/L, on the Prandtl number and $\alpha(\downarrow 0)$ have been suppressed.

In fig. 5 we plot $\lambda^{(q)}$ versus $k_{\perp}$ for the hard turbulence calculation described in section 3. The straight line is the $-11/3$ power law predicted by (40). A sensible inertial range appears to exists, in spite of the fact that

$$\mathrm{Re}_{\mathrm{T}} \approx 50, \tag{41}$$

i.e. the Taylor based Reynolds number Re_{T} is relatively small. The corresponding one-dimensional Fourier spectrum which is plotted in fig. 6 shows no indication of an inertial range.

At this point it is unclear why the empirical eigenfunctions appear to play such an essential role in describing the inertial range. To underline this concern we observe that for any admissible set of orthonormal functions, say $\{\psi^{(n)}(x)\}$, we can write

$$v = \sum_n b_n \psi^{(n)}(x) \tag{42}$$

and from this

$$\hat{e} = \sum_n \mu_n, \tag{43}$$

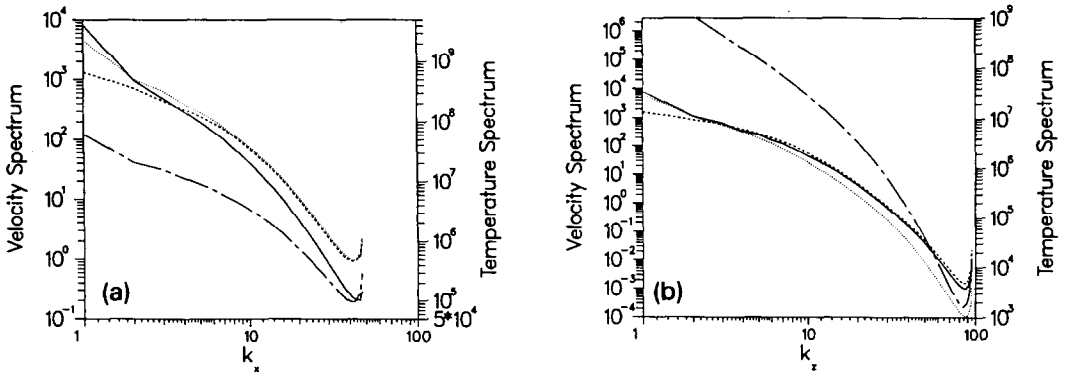

Fig. 6. (a) One-dimensional x-spectra. Long–short dashed curve is temperature. Continuous curve is u-velocity, short dash v-velocity and dots the w-velocity. (b) Same as (a) for z-spectra.

where

$$\mu_n = \langle b_n^2 \rangle_e = \langle (\psi^{(n)}, v)^2 \rangle_e. \tag{44}$$

Thus, μ_n can be interpreted as the average energy in the $\psi^{(n)}$ direction, in anology with our remarks about the meaning of λ_n. In particular, products of sinusoidal functions could be used for the $\{\psi^{(n)}(x)\}$. In that case μ_u is just $\mathscr{E}(k)$ and as already indicated this does not give rise to an inertial range. The empirical eigenfunctions therefore appear to perform a better job in organizing the spectra.

To gain some insight on a possible reason for this we note that $\hat{e}/H^3$ defines an average rms velocity for the fluctuating flow. Therefore $\hat{e}/H\nu^2$ is the square of a Reynolds number. Thus,

$$\mathrm{Re}^2 = \sum_n \mu_n/\nu^2 H = \sum_n \mathrm{Re}_n^2, \tag{45}$$

i.e. we can interpret each energy μ_n in terms of a corresponding Reynolds number.

On general principles we should expect an inertial range only when the relevant Reynolds is large enough. The KL procedure maximizes the energy in the principal modes thereby maximizing their corresponding Reynolds numbers, and leading to a relatively early inertial range. If we carry this line of reasoning further we might speculate that for any admissible basis set the corresponding μ_n will lead to an inertial range but only when the underlying Reynolds number of the problem becomes sufficiently high.

5. Approximate dynamical systems

To conclude this article, we show, at least briefly, how the empirical eigenfunction may be used to generate a low-dimensional dynamical description. In the notation of section 2 we write

$$v_N = \sum_{n=1}^{N} a_n(t)\phi^{(n)}(x) = P_N v. \tag{46}$$

If the fluid equations ar formally written as

$$\mathrm{d}v/\mathrm{d}t = F(v), \tag{47}$$

then the Galerkin procedure,

$$(\phi^{(k)}, \mathrm{d}v_N/\mathrm{d}t) = (\phi^{(k)}, F(v_N)), \quad k = 1, \ldots, N, \tag{48}$$

furnishes a straightforward means for generating a dynamical description.

This procedure has been applied to the Ginzburg–Landau (GL) equation [16,37,38] with remarkable success. Relatively few ordinary equations are able to faithfully describe the complex sequence of transitions to and from chaos found in the case of the GL equation. This material recently has been reviewed and [39] we do not survey it here. A similar approach was adopted for the Rayleigh–Bénard problem and is discussed in the dissertation of Tarman [40]. In this instance it was necessary to introduce an eddy viscosity, in the form of an added dissipation for the higher-order modes, to keep the number of equations down to a managable size. Aubry et al. [41] used a similar device, based on Heisenberg's eddy viscosity [42], in their model system for the boundary layer (also based on the empirical eigenfunctions).

A systematic development which leads to a generalized eddy viscosity follows from the method of slaved variables [43]. In this method a portion of the system of governing dynamical equation is replaced by algebraic equations, thus *slaving* (in time) certain of the dependent variables to the others, which are governed by the prescribed evolutionary equations. A mathematical framework for rigorously treating these ideas is contained in the study of *inertial manifolds* [44–47]. By definition an inertial manifold is one towards which solutions tend exponentially. In the remainder of this section we discuss recent work connecting empirical eigenfunctions and inertial manifolds [37]. More specifically we deal with the idea of approximate inertial manifolds [48,49].

If we write

$$\boldsymbol{v}_N^c = (1 - P_N)\boldsymbol{v}, \tag{49}$$

then

$$\boldsymbol{v} = \boldsymbol{v}_N + \boldsymbol{v}_N^c. \tag{50}$$

The dynamical system (47) may be divided in a corresponding fashion,

$$\mathrm{d}\boldsymbol{v}_N/\mathrm{d}t = P_N \boldsymbol{F}(\boldsymbol{v}_N + \boldsymbol{v}_N^c) = \boldsymbol{Q}_N(\boldsymbol{v}_N + \boldsymbol{v}_N^c), \tag{51}$$

$$\mathrm{d}\boldsymbol{v}_N^c/\mathrm{d}t = (1 - P_N)\boldsymbol{F}_N(\boldsymbol{v}_N + \boldsymbol{v}_N^c) = \boldsymbol{R}_N(\boldsymbol{v}_N + \boldsymbol{v}_N^c). \tag{52}$$

Inspection of this system leads us to the following heuristic argument: We can seek a basis $\{\boldsymbol{\phi}^{(n)}\}$ such that $R_N \to 0$ as $t \to \infty$. In this case we might hope that by taking the asymptotic initial data

$$\boldsymbol{v}_N^c \,|_{t=0} = 0, \tag{53}$$

then $\boldsymbol{v}_N^c \equiv 0$, so that

$$\mathrm{d}\boldsymbol{v}_N/\mathrm{d}t = \boldsymbol{Q}_N(\boldsymbol{v}_N). \tag{54}$$

The last system is equivalent to eq. (48), i.e. the Galerkin procedure.

In order to attempt to implement such a program we can start with the identity

$$\|\boldsymbol{v}\|^2 = \|\boldsymbol{v}_N\|^2 + \|\boldsymbol{v}_N^c\|^2, \tag{55}$$

and then search for a basis set $\{\boldsymbol{\phi}^{(n)}\}$ which minimizes the *error*, $\|\boldsymbol{v}_N^c\|^2$. More precisely, we want to minimize the ensemble average of this quantity,

$$\epsilon_N = \left\langle \|\boldsymbol{v}_N^c\|^2 \right\rangle. \tag{56}$$

The solution to the posed problem, viz. that the basis be optimal in the sense that (56) is minimized, is precisely the criterion leading to the empirical eigenfunctions, developed in section 2, as the required basis set.

In general, one might hope to improve on this procedure by retaining the influence of the neglected variables. Instead of neglecting $\boldsymbol{v}_N^c$ we can solve

$$\boldsymbol{R}_N(\boldsymbol{v}_N + \boldsymbol{v}_N^c) = 0 \tag{57}$$

for

$$\boldsymbol{v}_N^c = \boldsymbol{S}(\boldsymbol{v}_N) \tag{58}$$

and substitute into eq. (51) to obtain,

$$\mathrm{d}\boldsymbol{v}_N/\mathrm{d}t = \boldsymbol{Q}_N(v_N + \boldsymbol{S}(\boldsymbol{v}_N)). \tag{59}$$

This is the essence of the slaved variable method [43], and results in an approximation to the inertial manifold. In the course in doing this we are also introducing an added dissipation, or eddy viscosity, to the system.

Examination of the above discussion reveals that the strategy implicit in arriving at a reduced system has changed in passing from eq. (54) to eq. (59). In the first instance we sought a basis system, $\{\boldsymbol{\phi}^{(n)}\}$, which minimized the average error (56). On the other hand to arrive at eq. (59) we impose the condition (57). The latter implies that we should attempt to minimize $\| \boldsymbol{R}_N \|$ or, equivalently, $\| \dot{\boldsymbol{v}}_N^c \|$ instead of (56).

To develop this idea into a specific criterion, consider

$$\| \dot{\boldsymbol{v}} \|^2 = \| \dot{\boldsymbol{v}}_N \|^2 + \| \dot{\boldsymbol{v}}_N^c \|^2. \tag{60}$$

The desired criterion is that $\langle \| \dot{\boldsymbol{v}}_N^c \|^2 \rangle$ be minimized, or equivalently, that

$$E = \langle \| \dot{\boldsymbol{v}}_N \|^2 \rangle \tag{61}$$

be maximized. The objective is sufficiently close to the usual KL formulation so that we can state the procedure to follow in order to solve the new optimization problem. First, form the *acceleration* covariance [37]

$$\mathbf{L} = \langle \dot{\boldsymbol{v}} \otimes \dot{\boldsymbol{v}} \rangle. \tag{62}$$

The solution to the stated optimization problem is given by the eigenfunctions of $\mathbf{L}$, i.e. $\{\psi^{(n)}\}$ such that,

$$\mathbf{L}\psi = \lambda\psi. \tag{63}$$

The operator can be shown to be hermitian, non-negative and in certain cases can be proven to be square integrable. It then follows from Mercers theorem [50] that $\{\psi^{(n)}\}$ form a complete orthonormal basis. We can then appeal to the Karhunen–Loéve framework to show that

$$\dot{\boldsymbol{v}} = \sum_n b_n \psi^n, \quad b_n = (\psi^{(n)}, \boldsymbol{v}) \tag{64}$$

almost everywhere.

The basis set derived in this way, $\{\psi^{(n)}\}$, is optimal, by the above criterion, for use in the slaving method. To summarize, we split the system $(b_1, b_2, \ldots)$ into

$$\boldsymbol{v}_N \leftrightarrow \boldsymbol{b} = (b_1, \ldots, b_N), \tag{65}$$

$$\boldsymbol{v}_N^c \leftrightarrow \boldsymbol{b}^c = (b_{N+1}, \ldots), \tag{66}$$

according to some a priori criterion error bound,

$$\langle \| \boldsymbol{b}^c \|^2 \rangle < \epsilon. \tag{67}$$

The underlying dynamical system then may be written, in this notation, as

$$\mathrm{d}\boldsymbol{b}/\mathrm{d}t = \boldsymbol{T}(\boldsymbol{b}, \boldsymbol{b}^c), \quad \mathrm{d}\boldsymbol{b}^c/\mathrm{d}t = \boldsymbol{T}^c(\boldsymbol{b}, \boldsymbol{b}^c). \tag{68}$$

This splitting depends on the error criterion (67). The slaved system (approximate inertial manifold) is then obtained by neglecting the time derivative in the second part of (68),

$$\mathrm{d}\boldsymbol{b}/\mathrm{d}t = \boldsymbol{T}(\boldsymbol{b}, \boldsymbol{b}^c), \quad 0 = \boldsymbol{T}^c(\boldsymbol{b}, \boldsymbol{b}^c). \tag{69}$$

The above illustrates a somewhat different approach to the use of the empirical eigenfunctions. It has been applied to the GL equation [37], with an encouraging degree of success. Its application to other, more demanding cases, is an area of research.

6. Further comments

The use of the empirical eigenfunctions has been developed in a more or less a straightforward manner. But as implied in section 2 other weight functions, and more generally other norms, generate other basis sets of function. [Similar remarks apply to the averaging procedure.] An example of another norm appears in the previous section in which we discuss how one might optimally use the method of slaved variables to obtain an approximate inertial manifold. In this instance it is the norm of $\dot{v}$, instead of the velocity norm, eq. (3), which is used. Clearly there are limitless possibilities. In order to emphasize the smaller scales one might consider the eigenfunctions of the *enstrophy* kernel

$$\Omega_{ij} = \langle \omega_i(x)\omega_j(y)\rangle, \tag{70}$$

where ω is the vorticity. A referee suggested that the Reynolds stress be used to provide the eigenfunctions. [This then leads to a fourth-order tensor kernel.] Another, simpler, possibility which would emphasize the stress producing events would be the conditional sampling of snapshots at instants when the Reynolds stress meets some criterion threshold level. The velocity eigenfunctions would then be weighted to the events which lead to large Reynolds stresses.

It is possible to continue in this vein with many other possibilities. There is always a tradeoff between simplicity and the special requirements of a particular situation. The plan adopted here has been based on the straightforward approach, with the idea that this provides a framework which can be altered to suit some special needs.

While empirical eigenfunctions do lead to low-dimensional systems, certain somewhat technical problems do arise. Since the empirical eigenfunctions are non-local in space, non-linearities can lead to considerable interaction amongst modes. [In finite difference schemes interaction is limited since the Navier–Stokes equations are local.] This is also true for trigonometric expansions, however in this instance the fast Fourier algorithm greatly facilitates the calculations which arise. No comparable algorithm is known for the empirical eigenfunctions. The main thrust thus far in using the empirical eigenfunctions in simulations has been to use them to account for the large scale motions, i.e. for *large eddy simulation*. The small scales can then be treated in a variety of ways; say by the introduction of an eddy viscosity [51] or by a procedure such as EDQNM [52]. Ideally one would like to employ deliberations such as those discussed in section 4 in order to model the small scale behavior in a turbulent flow. This is a subject for future research.

Acknowledgement

The research here was supported by DARPA–URI under grant number N00014-86-K0754 and ONR grant number N00014-91-J-1588.

References

[1] K. Karhunen, Ann. Acad. Sci. Fennicae Ser. A 1 Math. Phys. (1946) 37.
[2] M.M. Loéve, Probability Theory (van Nostrand, Princeton, 1955).

[3] J.L. Lumley, The structure of inhomogeneous turbulent flows, in: Atmospheric Turbulence and Radio Wave Propagation, eds. A.M. Yaglom and V.I. Tatarski (Nauka, Moscow, 1967) pp. 166–178.
[4] J.L. Lumley, Stochastic Tools in Turbulence (Academic Press, New York, 1970).
[5] J.L. Lumley, Coherent structures in turbulence, in: Transition and Turbulence, ed. R.E. Meyer (Academic Press, New York, 1981) pp. 215–141.
[6] P. Moin and R.D. Moser, Characteristic eddy decomposition of turbulence in a channel, J. Fluid Mech. 200 (1989) 471–509.
[7] F.R. Payne and J.L. Lumley, Large eddy structure of the turbulent wake behind a circular cylinder, Phys. Fluids 10 (1967) S194–196.
[8] M.N. Glauser, S.J. Lieb and N.K. George, Coherent structure in axisymmetric jet mixing layer, Proc. 5th Symp. Turbulent Shear Flow, Cornell University (Springer, Berlin, 1985).
[9] P. Moin, Probing turbulence via large eddy simulation, AIAA paper 84-0174 (1984).
[10] L. Sirovich, Turbulence and the dynamics of coherent structures, I. Coherent structures, Q. Appl. Math. 45 (1987) 561–571.
[11] L. Sirovich, Turbulence and the dynamics of coherent structures. II. Symmetries and transformations, Q. Appl. Math. 45 (1987) 573–582.
[12] L. Sirovich, Turbulence and the dynamics of coherent structures. III. Dynamics and scaling, Q. Appl. Math. 45 (1987) 583–590.
[13] R.W. Preisendorfer, Principal Component Analysis in Meteorology and Oceanography (Elsevier, Amsterdam, 1988).
[14] R.B. Ash and M.F. Gardner, Topics in Stochastic Processes (Academic Press, New York, 1975).
[15] P.A. Devijver and J. Kittler, Pattern Recognition: a Statistical Approach (Prentice–Hall, Englewood Cliffs, 1982).
[16] L. Sirovich and J.D. Rodriguez, Coherent structures and chaos: a model problem, Phys. Lett. A 120 (1987) 211–214.
[17] L. Sirovich, M. Maxey and H. Tarman, An eigenfunction analysis of turbulent thermal convection, In: Post-conference Proceedings, ed. B. Launder (Springer, Berlin, 1988).
[18] L. Sirovich, S. Balachandar and M.R. Maxey, Simulations of turbulent thermal convection, Phys. Fluids A 1 (1989) 1911–1914.
[19] S. Balachandar, M.R. Maxey and L. Sirovich, Numerical simulation of high Rayleigh number convection, J. Sci. Comput. 4 (1989) 219–236.
[20] L. Sirovich and H. Park, Turbulent thermal convection in a finite domain. I. Theory, Phys. Fluids A 2 (1990) 1649–1658.
[21] H. Park and L. Sirovich, Turbulent thermal convection in a finite domain. II. Numerical results, Phys. Fluids A 2 (1990) 1659–1668.
[22] K.S. Ball, L. Sirovich and L.R. Keefe, Dynamical eigenfunction decomposition of turbulent channel flow, Int. J. Num. Meth. Fluids, in press.
[23] L. Sirovich, M. Kirby and M. Winter, An eigenfunctions approach to large scale transitional structures in jet flow, Phys. Fluids A 2 (1990) 127–136.
[24] P.G. Drazin and W.H. Reid, Hydrodynamic Stability (Cambridge Univ. Press, Cambridge, 1981).
[25] B. Castaing, G. Gunaratne, F. Heslot, L. Kadanoff, Al Libchaber, S. Thomae, X.-Z. Wu, S. Zaleski and G. Zanetti, Scaling of hard thermal turbulence in Rayleigh–Bénard convection, J. Fluid Mech. 204 (1989) 1–30.
[26] A.E. Deane and L. Sirovich, A computational study of Rayleigh–Bénard convection. I. Rayleigh number dependence, J. Fluid Mech. 222 (1991) 231.
[27] L. Sirovich and A.E. Deane, A computational study of Rayleigh–Bénard convection. II. Dimension considerations, J. Fluid Mech. 222 (1991) 251.
[28] A.N. Kolmogorov, C.R. Acad. Sci. URSS 30 (1941) 301–538.
[29] H. Tennekes and J.J. Lumley, A First Course in Turbulence (MIT Press, Cambridge, 1972).
[30] P.W. Bridgman, Dimensional Analysis, 2nd Ed. (Yale University Press, New Haven, 1931).
[31] A.N. Kolomogorov, J. Fluid Mech. 13 (1962) 82.
[32] B.B. Mandelbrot, J. Fluid Mech. 62 (1974) 331.
[33] U. Frisch, P.L. Sulem and M. Nelkin, J. Fluid Mech. 87 (1978) 219.
[34] U. Frisch, in: Nonlinear Dynamics, ed. R. Helleman (NY Acad. Sci., New York, 1980) 357, 359.
[35] B. Knight and L. Sirovich, Kolmogorov inertial range for inhomogeneous turbulent flows, Phys. Rev. Lett. 65 (1990) 1356.
[36] J. Kim, P. Moin and R. Moser, J. Fluid Mech. 177 (1987) 133.
[37] L. Sirovich, B.W. Knight and J.D. Rodriguez, Optimal low dimensional dynamical approximations, Q. Appl. Math. 48 (1990) 555–548.
[38] J.D. Rodriguez and L. Sirovich, Low-dimensional dynamics for the complex Ginzburg–Landau equation, Physica D 43 (1990) 77–86.

[39] L. Sirovich, Empirical eigenfunctions and low dimensional systems, in: New Perspectives in Turbulence, ed. L. Sirovich (Springer, Berlin), to be published.
[40] H. Tarman, Dissertation, Brown University, Providence (1989).
[41] N. Aubry, P. Holmes, J.L. Lumley and E. Stone, The dynamics of coherent structures in wall region of a turbulent boundary layer, J. Fluid. Mech. 192 (1988) 115–175.
[42] W. Heisenberg, Ang. Physik 124 (1948) 628.
[43] N.G. van Kampen, Elimination of fast variables, Phys. Rep. 124 (1985) 69–160.
[44] C. Foias, G.R. Sella and R. Temam, Inertial manifolds for nonlinear evolutionary equations, J. Differential Equations 73 (1988) 309–353.
[45] J. Mallet-Paret, and G.R. Sell, Inertial manifolds for reaction–diffusion equations in higher space dimensions, J. Am. Math. Soc. 1 (1988) 805–866.
[46] P. Constantin, C. Foias, B. Nicolenko and R. Temam, Integral manifolds and inertial manifolds for dissipative partial differential equations, Applied Math. Sci. (Springer, Berlin, 1989).
[47] P. Constantin, Remarks on the Navier–Stokes equations, in: New Perspectives in Turbulence (Springer, Berlin, 1990).
[48] E. Titi, On approximation inertial manifolds to the Navier–Stokes equations, Math. Sci. Inst. Rep., Cornell University, Ithaca (1989).
[49] D. Foias, O.P. Manley and R. Teman, Sur l'interaction des petits et grands tourbillars dans les ecoulements turbulents, C. R. Acad. Sci. Paris Ser. I 305 (1987) 497–500.
[50] F. Riesz and B.Sz. Nagy, Functional Analysis (Ungar, New York, 1955).
[51] H. Tarman, Analysis of turbulent thermal convection, Thesis, Brown University, Providence (1989).
[52] H. Park and L. Sirovich, Closure models for turbulent convection based on the empirical eigenfunctions, in preparation.